

# A Dataset for Evaluating Blood Detection in Hyperspectral Images

Michał Romaszewski<sup>†</sup>, Przemysław Głomb, Arkadiusz Sochan, Michał Cholewa

Institute of Theoretical and Applied Informatics, Polish Academy of Sciences

Bałycka 5, 44-100 Gliwice, Poland

Email: {mromaszewski, pglomb, asochan, mcholewa}@iitis.pl

Telephone: +48 32 2317319

(<sup>†</sup>Corresponding author)

## Abstract

The sensitivity of imaging spectroscopy to hemoglobin derivatives makes it a promising tool for detecting blood. However, due to complexity and high dimensionality of hyperspectral images, the development of hyperspectral blood detection algorithms is challenging. To facilitate their development, we present a new hyperspectral blood detection dataset. This dataset, published in accordance to open access mandate, consist of multiple detection scenarios with varying levels of complexity. It allows to test the performance of Machine Learning methods in relation to different acquisition environments, types of background, age of blood and presence of other blood-like substances. We explored the dataset with blood detection experiments. We used hyperspectral target detection algorithm based on the well-known Matched Filter detector. Our results and their discussion highlight the challenges of blood detection in hyperspectral data and form a reference for further works.

**Keywords:** Hyperspectral imaging; Blood detection; Target detection; Matched Filter;

## 1 Introduction

Detecting blood is crucial in the process of gathering evidence in accident or crime scene investigations [1]. The focus of this paper is the use of Hyperspectral Imaging (HSI) or Imaging Spectroscopy (IS) for detection and identification of blood. Typically blood is identified using chemical tests which change color [2], fluoresce [3] or luminesce [4] when they come in contact with blood stains. However, these chemicals must be locally applied in the area where blood stains are present and they can lead to a loss of evidence or they can interfere with other procedures [4]. Therefore, application of imaging spectroscopy for identifying and analysing blood properties is a particularly promising field of study [1], related to a broader problem of hyperspectral target detection [5]. In addition, the ability to locate blood with imaging technique can be helpful to investigators.

HSI has many applications such as remote sensing of vegetation [6] food quality control [7], aiding in art conservation [8] or detection of gunshot residue [9]. The difficulty of applying HSI for blood detection depends on such factors as acquisition conditions, background complexity and spectral variability of blood stains. This makes hyperspectral blood detection task particularly interesting from the perspective of applied vision and Machine Learning methods. However, testing such methods requires reference data that takes into account the typical challenges they face: various lighting at the acquisition site, the presence of shadows, materials of different texture and colour as the background, differences in the angle and distance of the camera from the imaged surface or changes in spectra between consecutive acquisitions.

Therefore, to facilitate creation, testing and comparison of blood detection algorithms, in this paper we would like to introduce a new dataset for blood detection in hyperspectral images. The datasets consists of multiple scenarios presented in the form of hyperspectral images of a mock-up scene. The intention behind these scenarios is to reflect the diversity and varying levels of detection difficulty. To facilitate the use of our research, the

dataset along with source code and ground truth maps required to replicate our results are available on-line under an open licence. To our knowledge, there is currently no publicly available dataset of a similar nature.

Along with this dataset we provide reference target detection experiments which are intended to illustrate the problem and highlight its challenges. The proposed detection algorithm is based on a well known statistical detector, namely a Matched Filter (MF), following the reasoning presented in [10] that a reasonable approach is to use detector algorithms with good performance and well-understood theoretical properties.

This paper is organised as follows: Sec. 2 shortly introduces the problem of hyperspectral target detection. Sec. 3 describes the new hyperspectral dataset. Sec. 4 describes measures of performance used in our experiments, presents an example of target detection and introduces the proposed detection algorithm. Experiments and results are presented in the Sec. 5 and discussed in Sec. 6. Finally, conclusions are presented in Sec. 7.

### 1.1 Related work

Visibility of hemoglobin derivatives such as oxyhemoglobin (oxyHb) and methemoglobin (metHB) in hyperspectral data makes hyperspectral imaging useful in a range of applications related to medical diagnosis [11]. The presence of these derivatives corresponds in particular to characteristic peaks in reflectance spectra, for example in wavelengths  $\sim 542$  nm and  $\sim 576$  nm referred as  $\alpha$  and  $\beta$  bands (see Fig. 1). These data features are mostly consistent for both human and animal blood [12] and can be applied e.g. for detection of blood and estimation of hemoglobin concentration in fish muscle [13]. The process of hemoglobin degradation corresponds to observable changes in reflectance spectra in range 450–800 nm [14] which can be used to identify and estimate the age of blood [15].

Hyperspectral imaging is used for analysing various forensic traces such as fingermarks, drugs, inks, tapes, firearm propellant or fibers, but sensitivity to hemoglobin makes it particularly

suitable for analysis of blood in forensic scenes [16]. An important research problem lies in distinguishing between blood and other substances. A study of such problem is presented in [17] where authors compare spectral characteristics of blood and nine types of non-blood substances such as tomato sauce or red wine and conclude that blood is significantly different from them. Another interesting application lies in finding and identification of blood stains in the field, which corresponds to detection in an unknown and diverse acquisition environment. For example in [16] authors created a simulated crime scene in order to estimate the age of blood stains, this research was continued and extended in [18]. In [19] a simulated scene was used to perform a preliminary verification of two anomaly detection algorithms. Some works such as [20] or [21] try to combine these approaches with experiments involving detection of blood in presence of other substances on fabric backgrounds of different colour.

## 2 Hyperspectral target detection

We treat the task of detecting blood in the imaged scene as a hyperspectral target detection problem. The aim of the detector is to find hyperspectral pixels where searched target spectrum is visible.

### 2.1 Likelihood ratio detectors

We treat a hyperspectral image as a set of pixels  $\mathbf{x} \in \mathcal{X} \subset \mathbb{R}^{N \times d}$ , where  $N$  is the number of pixels in the image and  $d$  is the number of bands. Following the introduction presented in [5], we can describe the task of hyperspectral target detection as follows: given an example pixel  $\mathbf{x}$ , our goal is to choose between two competing hypotheses:

$$\begin{aligned} H_0 &: (\text{target absent}) \\ H_1 &: (\text{target present}). \end{aligned}$$

Let  $p(\mathbf{x}|H_0)$  and  $p(\mathbf{x}|H_1)$  be conditional probability density functions under the two hypotheses. Then, the likelihood ratio (also called the detection statistics) is given by  $\Lambda(\mathbf{x}) = \frac{p(\mathbf{x}|H_0)}{p(\mathbf{x}|H_1)}$ . Given some threshold  $\eta$ , if the likelihood ratio  $\Lambda(\mathbf{x}) > \eta$ , We accept  $H_1$  hypothesis as true.

Selection of the detection method is based on the premise that we are looking for full-pixel targets. Since detectors based on Gaussian probability models often lead to good performance, as described in [5] or [10], a reasonable starting point could be the assumption that both the target and the background spectra can be described by multivariate Gaussian distributions. This leads to detectors based on likelihood ratio test, which by the Neyman–Pearson lemma is the most powerful statistical test.

#### 2.1.1 Quadratic detector

Following [5], a detection problem can be represented in the form of the following hypotheses:

$$\begin{aligned} H_0 &: \mathbf{x} \sim \mathcal{N}(\boldsymbol{\mu}_0, \boldsymbol{\Gamma}_0) \\ H_1 &: \mathbf{x} \sim \mathcal{N}(\boldsymbol{\mu}_1, \boldsymbol{\Gamma}_1), \end{aligned} \quad (1)$$

where target and background classes follow the multivariate Gaussian distributions, vector  $\mathbf{x}$  is the pixel under test (PUT), vector  $\boldsymbol{\mu}_0$  and matrix  $\boldsymbol{\Gamma}_0$  are the mean and covariance matrix of the background, vector  $\boldsymbol{\mu}_1$  and matrix  $\boldsymbol{\Gamma}_1$  are the mean and

covariance matrix of targets. Provided they are all known in advance, we can use the Quadratic Detector [5] (QD):

$$\begin{aligned} y &= D_{\text{QD}}(\mathbf{x}, \boldsymbol{\mu}_0, \boldsymbol{\mu}_1, \boldsymbol{\Gamma}_0, \boldsymbol{\Gamma}_1) \\ &= (\mathbf{x} - \boldsymbol{\mu}_0)^T \boldsymbol{\Gamma}_0^{-1} (\mathbf{x} - \boldsymbol{\mu}_0) - (\mathbf{x} - \boldsymbol{\mu}_1)^T \boldsymbol{\Gamma}_1^{-1} (\mathbf{x} - \boldsymbol{\mu}_1), \end{aligned} \quad (2)$$

which compares the Mahalanobis distance of the pixel under test to means of target and background distribution.

#### 2.1.2 Matched filter

The use of QD is subject to very strong assumptions in the form of knowledge about the distribution of the target and the background in the image. If we limit our knowledge to the target spectral signature  $\boldsymbol{\mu}_1$ , the remaining distribution characteristics could be estimated from data. If we assume that the target and background classes have the same covariance matrix  $\boldsymbol{\Gamma}_0 = \boldsymbol{\Gamma}_1 \equiv \boldsymbol{\Gamma}$ , the use of Neyman–Pearson lemma leads us to the Matched Filter (MF) detector:

$$y = D_{\text{MF}}(\mathbf{x}, \boldsymbol{\mu}_0, \boldsymbol{\mu}_1, \boldsymbol{\Gamma}) = \frac{(\mathbf{x} - \boldsymbol{\mu}_0)^T \boldsymbol{\Gamma}^{-1} (\boldsymbol{\mu}_1 - \boldsymbol{\mu}_0)}{(\boldsymbol{\mu}_1 - \boldsymbol{\mu}_0)^T \boldsymbol{\Gamma}^{-1} (\boldsymbol{\mu}_1 - \boldsymbol{\mu}_0)}. \quad (3)$$

## 3 Blood detection dataset

Considering a scenario where HSI could be used for blood detection at the accident or crime scene, we propose the following assumptions:

1. The final goal of the experiment is to detect targets i.e. blood stains in the image, by assigning a positive label to pixels where blood is visible and negative label to other pixels.
2. We consider the use of supervised algorithms that use a training set of representative blood patterns. These training patterns should represent general properties of the target spectrum and in particular, should come from an external source e.g. a spectral library.
3. The detector shouldn't require any specific information about the background of the image i.e. training data consists only of target spectra.
4. Blood traces in the image are typically visible as groups of pixels. However, these target pixels do not have to be pure i.e. target spectrum is likely to be mixed with background spectra.

In accordance with these assumptions, we formulated a number of target detection scenarios. A scenario is associated with a fragment of the prepared mock-up scene with varying background materials of different colour, shape and composition. Blood traces of varying size and shape were placed in the scene along with a set of visually similar substances such as artificial blood, tomato juice or red paints. As a result, the expected difficulty of detection task varies between scenarios: from a relatively simple environment where the majority of targets is located on a uniform, white background to complex environments with varied backgrounds and blood-like substances. Available images represent multiple acquisitions over a period of three weeks, with a particular focus on the first two day of acquisition which allows to observe the impact of time-induced changes in the scene on detection performance.

### 3.1 Description of the dataset

The dataset presented in this paper consists of hyperspectral images of six fragments of the scene, representing different detection scenarios. Individual scenes are presented in the Fig. 1 and assigned the letters A-F. Their description and motivation are as follows:

#### 3.1.1 Scene A „Head”

Traces of real and artificial blood are located on white materials (bandage, fragment of a white sheet) and on the fragment of the blue shirt on the left side. The background in the immediate vicinity of the blood traces is fairly uniform, but in the far background of the image there is a mixture of plastics and organic substances (fruits and vegetables) of different colour.

The scene is intended as a relatively easy detection scenario, with the majority of targets located on a white background. The main challenge lies in the need to detect substances on two significantly different backgrounds (white and blue) and to distinguish between blood and artificial blood.

#### 3.1.2 Scene B „Shirt”

On this scene, traces of real and artificial blood are located on the blue material of the thick, cotton shirt put on a mannequin. In addition, part of the „Head” scene is also visible.

This scenario is more complex than scenario A, allowing to examine the effectiveness of blood detection on a dark background in presence of cloth fabric bends and resulting shadows.

#### 3.1.3 Scene C „Knife”

On this scene, traces of real and artificial blood are present on the blade and handle of the knife and in its vicinity. The scene allows to test detection in presence of substances of significantly different type and colour (metal blade, plastic handle, mixture of fabrics).

#### 3.1.4 Scene D „Splash”

This scene contains a blood splash pattern on a white cotton shirt. The splash was prepared by placing the blood sample on a plastic container located in the centre of the scene, and hitting it with a hard object. The traces form a circular pattern while its geometrical centre stays mostly clean.

Apart from detection problem, the method of application allows to experiment with spatial properties of the blood splashes e.g. determining the location of the geometric centre of the splash or estimating its shape.

#### 3.1.5 Scene E „Comparison”

This scene contains blood and five blood-like substances on eight different backgrounds, which are a mixture of fabrics, wood, plastic and metal, some of them red. They were arranged in uniform, vertical stripes while blood along with five blood-like substances were placed on them in horizontal stripes.

The purpose of the scenario is to test the detector in a challenging and diverse environment with many materials optically similar to detected targets.

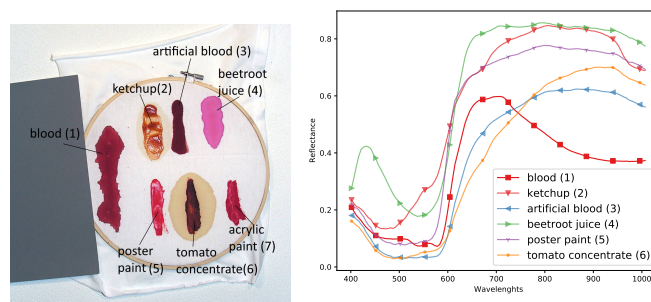
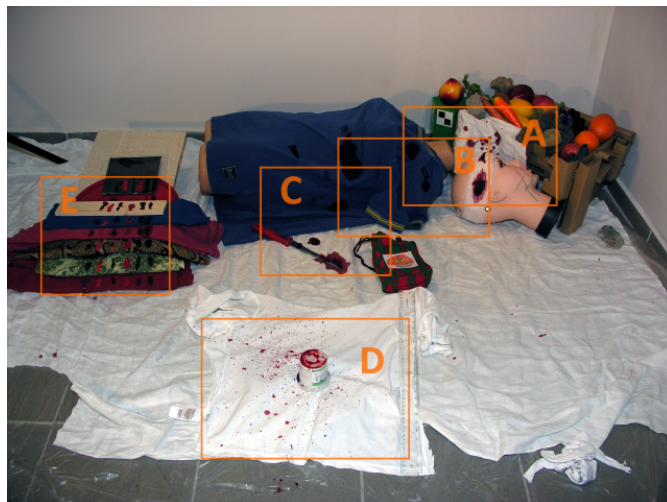


Figure 1: Top: the mock-up scene with blood patterns and annotated scenarios A-E. Left: the scenario F „Frame”. Right: spectra of blood and blood-like substances from the scenario F.

#### 3.1.6 Scene F „Frame”

This scene contains blood and six blood-like substances on a piece of a white fabric. The fabric was stretched on a wooden frame to minimise the occurrence of bends. This scene is intended as a source of blood spectra for experiments and was acquired multiple times in the space of three months and also with different types of hyperspectral cameras.

### 3.2 Preparation of the scene

After preparing the mock-up scene, the blood-like substances were applied first. Then, three blood samples obtained from authors in a sample collection facility were applied. Each sample had a volume of 15ml so in total 45ml were used. Blood samples did not contain anticoagulant, and were applied to the scene in about 10 minutes after being taken. The approximate age of samples in images is presented in the Tab. 2

Acquisitions were carried out over a period of multiple weeks. With one exception, all acquisitions were performed in the same room without windows, with stable humidity and temperature of about 15 degrees Celsius.

Elements of scenes A-E were not moved in this time, although the camera and lights were adjusted in most of the acquisitions.

The frame denoted as scene F was moved outside of the laboratory in the second day to be used for reference acquisitions with different hyperspectral camera and was returned later. This reference acquisition is denoted as  $F(2k)$  in Tab. 2, however, the actual spectra values in the data cube were interpolated to match the rest of images in the dataset. In addition, in the first day the frame was placed in the mock-up scene in order to acquire its image in similar lighting conditions to other images in the dataset. This image is denoted as  $F(1s)$ .

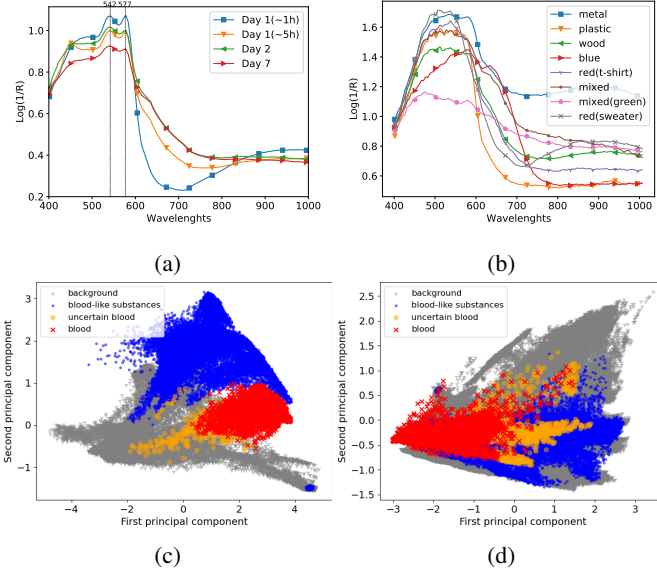


Figure 2: Panel (a): differences between averaged blood spectra captured over the week. The marked frequencies, corresponding to the so-called  $\alpha$ - and  $\beta$ -bands, are associated with the spectral response of haemoglobin. Panel (b): Differences between blood spectra on different backgrounds in the scenario  $E(I)$ . Bottom: PCA plots where data is projected on first two principal components in scenarios  $F(I)$  on panel (c) and  $E(I)$  on panel (d).

### 3.3 Hyperspectral acquisition

Hyperspectral data acquisition was performed with Surface Optics SOC710 camera. This camera records spectra at VNIR range 377–1046nm; the output image has dimensions  $696 \times 520$  with 128 bands and 12 bit dynamic range. The camera is equipped with sensor line translation unit and can be used from static stand as a conventional camera (i.e. it does not require mechanical translation of the observed sample or rotary stand, as in traditional ‘push broom’ hyperspectral cameras). The lighting was provided with four halogen lamps and adjusted for each scenario separately, so that most of the dynamic range of the camera was used and image saturation is avoided. Captured hyperspectral images were subject to a standard calibration procedure, including: the removal of a dark frame, spectral and radiometric calibration as well as reflectance normalization using the calibration panel. Images in scenarios  $B$  and  $C$  images do not contain calibration panel, therefore reflectance calibration was performed based on a separate acquisition and verified by comparing spectra with other images.

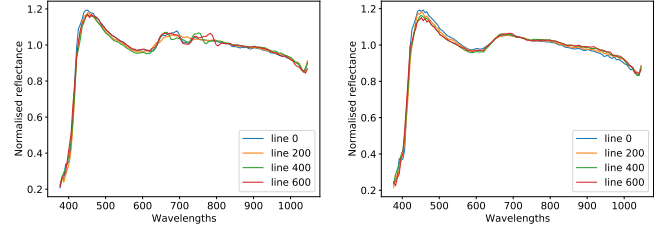
#### 3.3.1 Reflectance correction

We observed that the spectra from the camera contain distortions that correlate with pixel horizontal position. These distortions have a constant characteristic and are probably a result of equipment error. To correct these distortions, we use a reference hyperspectral image of grey Munsell Color panel (Munsell Notation: N5) with known spectral characteristics.

Let  $G_{\text{ref}}$  be a hyperspectral cube of the panel image. For every a  $i, j$ -th pixel  $w_{\text{ref}}^{ij} \in \mathbb{R}^d$  in the image  $G_{\text{ref}}$ , we use the known image spectrum  $\tilde{w}_{\text{ref}}$ , to compute this pixel residue:

$$r_{\text{ref}}^{ij} = w_{\text{ref}}^{ij} - \tilde{w}_{\text{ref}}.$$

Then, for every pixel  $p_{\text{ref}}^{ij} \in \mathbb{R}^d$  in the corrected image  $P_{\text{ref}}$ , a



(a) Before reflectance correction (b) After reflectance correction

Figure 3: Visualisation of the impact of reflectance correction on reference image spectra. The imaged area was a white paper sheet. Each spectrum represents the mean spectrum of 100 pixels from one horizontal line in the image, normalised by dividing this spectrum by its median. In panel (a), before correction distortions in range 600–850nm are visible. In panel (b), after correction these distortions were removed.

corrected pixel is computed as

$$p_{\text{ref}}^{ij} = P_{\text{ref}}^{ij} - r_{\text{ref}}^{ij} \frac{\delta_p^{ij}}{\delta_w^{ij}},$$

where  $\delta_p^{ij}$  is the median of the pixel  $p_{\text{ref}}^{ij}$  and  $\delta_w^{ij}$  is the median of a panel pixel  $w_{\text{ref}}^{ij}$ . Corrected pixels form a corrected image  $P'_{\text{ref}}$ . Visualisation of the correction effect is presented in Fig. 3

### 3.4 Dataset annotation

Annotation of blood and blood-like substances was performed by authors. The criteria of assigning a pixel to a class was the prior knowledge about where the substance was applied, visibility of the substance in the image and responses of multiple detectors searching for spectra selected in the image. In some cases such as the tomato concentrate in Fig. 2 (denoted as class 6) the visible stain can be divided into two clearly different areas of intensity. For substances other than blood, only the more pronounced area was designated. For the blood class, first the correctness of annotation was verified by comparing a subset of images annotated by multiple experts. It was determined that the majority of differences correspond to areas about 1 pixel thick located on the edges of stains. To facilitate this, blood was assigned two classes: Pixels where blood is clearly visible were annotated as class 1. Pixels where blood occurrence is uncertain or indistinct were annotated with a separate class denoted as class 8 („uncertain blood”).

### 3.5 Spectral properties of blood

The impact of the day of acquisition on blood spectra is presented in Fig. 2. Results seem consistent with reference literature [14]. During the first day spectra change significantly due to oxidation of hemoglobin while changes in the following days are minor. This suggests that detection of fresh blood is a more complex problem due to additional spectra variability. The Fig. 2 also presents differences in blood spectra resulting from different background materials. Spectra seem to be strongly affected by different backgrounds. Spectra plotted in these figures were averaged over the image.



### 3.6 Dataset and code availability

The dataset consist of 14 hyperspectral images in ENVI format, each  $\sim 180\text{MB}$  in size, along with documentation and target annotations. In accordance with open-access mandate, the dataset is publicly available on-line<sup>1</sup> under an open license. In addition, code for experiments performed in this paper are also available under GNU General Public License<sup>2</sup>

## 4 Methods

This section starts by introducing measures of detection performance used when presenting our results. To illustrate them, a simple example is provided where the Matched Filter (MF) detector, described in Sec. 2, is applied to one of the images from our dataset. Finally, a MF-based detection algorithm used in our experiments is presented.

### 4.1 Evaluation of detector effectiveness

Given a detector with known detection statistics for some value of threshold  $\eta$ , the decision made by a detector can be represented as a Confusion Matrix (CM), whose diagram is presented as the Tab. 1. CM divides detection results between four types of outputs: True Positives (TP) are pixels where target was correctly detected, False Positives (FP) refer to pixels where target was detected incorrectly, True Negatives (TN) are pixels where target is correctly not detected and False Negatives (FN) refer to pixels where target was present but not detected. The confusion

	actual $H_1$	actual $H_0$
predicted $H_1$	TP	FP
predicted $H_0$	FN	TN

Table 1: A Confusion Matrix

matrix is the basis to define common metrics used to evaluate detector's performance: True Positive Rate,  $\text{TPR} = \frac{\text{TP}}{\text{TP} + \text{FN}}$ , False Positive Rate,  $\text{FPR} = \frac{\text{FP}}{\text{FP} + \text{TN}}$ , Recall =  $\frac{\text{TP}}{\text{RP} + \text{FN}}$  and Precision =  $\frac{\text{TP}}{\text{TP} + \text{FP}}$ .

However, it is not obvious how to set the threshold  $\eta$ , as increasing its value increases the probability of correct detections  $P_{TP}$  but at the same time increases the probability of false positive detection (false alarms)  $P_{FP}$ . Assessment of this trade-off leads to the standard performance metrics for detectors, namely the receiver operating characteristics (ROC) curve [5]. ROC curve plots the probability  $P_{TPR}(\eta)$  versus the probability  $P_{FPR}(\eta)$  for possible values of the threshold  $\eta$ . The performance of the detector can be expressed as a numerical value in the form of the Area Under Curve (AUC) statistics, which assumes values in the range  $\langle 0, 1 \rangle$ , with  $\text{AUC} = 1.0$  corresponding to „oracle” detector that assigns highest values of detection statistics to target pixels and  $\text{AUC} = 0.5$  corresponding to a detector that detects targets „at random”.

Imbalance in target and background class sizes, in particular when the number of correct detections is small in comparison to the number of background pixels, leads to a serious bias towards the majority (background) class. This can make ROC curves less informative for comparing detectors, as values of  $\text{AUC}_{\text{ROC}}$  for evaluated detectors become similar.

<sup>1</sup>Dataset DOI: 10.5281/zenodo.3984905

<sup>2</sup>Source Code: [https://github.com/iitis/HSI\\_blood\\_detection.git](https://github.com/iitis/HSI_blood_detection.git)

For such skewed datasets, Precision-Recall (PR) curves, that plot values of Precision( $\eta$ ) versus Recall( $\eta$ ), can give a more informative picture of an algorithm's performance [22]. However, when comparing two detectors, both AUC and PR measures give similar results [22].

### 4.2 Detection scenarios

Regarding likelihood ratio detectors presented in the Sec. 2.1, we can define the following scenarios of their use:

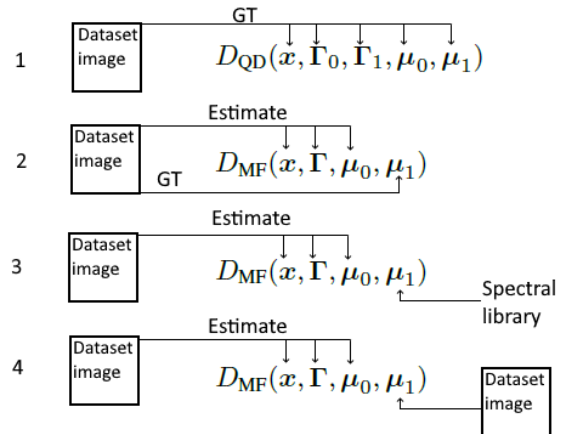


Figure 4: A schema of detection scenarios. „GT” denotes the use of ground truth information. „Estimate” denotes values estimated globally from image data.

1. Target and background means and covariance matrices from the processed image are supplied to the Quadratic Detector, given by the Eq. (2).
2. Target and background means from the processed image are supplied to the MF detector given by the Eq. (3) while, following the assumption from Sec. 2.1.2, the common covariance matrix  $\Gamma$  is the global sample covariance matrix of the image. We call this scenario the *Ideal MF*, due to the fact that the exact target spectrum  $\mu_1$  is known.
3. The MF detector is supplied with a common covariance matrix  $\Gamma$  estimated as the global sample covariance matrix and the background mean  $\mu_0$  estimated as mean spectrum of all pixels in the image. Mean target spectrum  $\mu_1$  is taken from an external source e.g. a spectral library.
4. The scenario is similar to the previous one, but the mean target spectrum  $\mu_1$  is a sample mean spectrum of the blood class from another image in the dataset. We call this an *Inductive MF* scenario, due to its similarity to the problem of inductive learning in ML, where a model trained on a set of representative training examples is used to make predictions.

Schemas of these scenarios are presented in Fig. 4. In our experiments we focus on the last three scenarios, treating the Scenario 3 as our main experiment and the rest as a reference.

### 4.3 Detection example

Referring to the scenarios presented in Sec. 4.2, we present an example experiment, where the MF detector, given by Eq 3 is applied to one of the images in the dataset, namely the scene  $E(I)$ .

Background mean  $\mu_0$  and covariance matrix  $\Gamma$  are computed as sample mean and sample covariance matrix of the whole image. The target mean  $\mu_1$  is either a mean of the blood class pixels i.e. the *Ideal MF*, the mean of the blood class pixels from the image  $F(1s)$  i.e. the *Inductive MF* or the blood spectrum from an external spectral library provided by authors of [14].

Results of this experiment are presented in the Fig. 5. The panel (a) presents the ground truth - blood class is denoted with red colour. Panels (b) and (c) present detection performance in the form of (respectively) PR and ROC curves, with aggregated performance expressed as the Area Under Curve (AUC). As expected, the performance is higher in the „Ideal MF” scenario.

Panel (d) presents detection statistics of the *Ideal MF* as a heat map. We can see that areas corresponding to blood location are visibly darker. The two remaining plots present a coloured detection map for *Ideal MF* and *Inductive MF* scenarios. This map is obtained by setting the threshold  $\eta$  (see Sec. 2) to the actual ratio of blood pixels in the image, i.e.  $\eta = \frac{\text{no. blood pixels}}{\text{no. all pixels}}$ . Colours in the map correspond to True Positive detections as well as two types of errors (FN, FP). As we can see, the detection map presented in the panel (e) fairly resembles the ground truth. Notable errors include FP detection of class 3 (artificial blood, the fifth class from the left of GT), visible in the top area of the image. Errors in the last panel are more numerous, which is consistent with lower performance in the *Inductive MF* scenario in Panel (b).

#### 4.4 Detection algorithm

The detection algorithm used in our experiments is based on the Matched Filter (MF) detector, described in Sec. 2. The motivation for this algorithm is the discussion provided in [10] as well as two observations: a high performance of the *Ideal MF* detector trained on the mean spectra of blood in the image (see example in the Sec. 4.3) and the fact that many pixels with highest values of MF detector score seem to be True Positives (TP).

The general idea is to use a two-stage detector. In the first stage an MF detector will be used to locate a subset of pixels in the image that are likely from the target class. A mean spectrum of these pixels will be used to create a new „local” estimation of a target spectral signature. This new target signature will be used in the second stage, to train a final MF detector that will output pixel detection scores. A more formal description of this algorithm is provided as Algorithm 1

## 5 Experiments and results

The experiment applies the detection Algorithm 1 to images from our dataset. The algorithm requires a training data, namely a searched target spectrum. These spectra are taken from spectral library provided by authors [14]. The library contains blood spectra from days 0-29. To standardise spectral ranges, wavelengths and the number of bands between the library and dataset images, we removed bands [0-4] and [122-128] from dataset images and used linear interpolation on library spectra to obtain spectra corresponding with wavelengths from our camera. In addition, three noisy bands [48, 49, 50] were also removed from images leaving 113 bands.

In order to compensate for uneven illumination of the imaged scene, hyperspectral cubes were normalised by dividing every hyperspectral pixel by its median.

```

Data: Target spectral signature  $\mu_1 \in \mathbb{R}^d$ , Array of pixels
          $\mathbf{X} \in \mathbb{R}^{K \times d}$ , parameter N
Result: Pixel detection statistics  $\mathbf{Y} \in \mathbb{R}^K$ 
/* Stage 1
estimate  $\mu_0, \Gamma$  from  $\mathbf{X}$ 
 $\mathbf{Y} \leftarrow \emptyset$ 
for pixel  $x$  in  $\mathbf{X}$  do
|  $\mathbf{Y} \leftarrow D_{MF}(x, \mu_0, \mu_1, \Gamma)$ 
end
/* Stage 2
 $a \leftarrow \text{argsort}(\mathbf{Y})$ 
/*  $\mathbf{X}[a]$  denotes sorting  $\mathbf{X}$  by  $a$ 
 $\mathbf{X}' \leftarrow N$  first values of  $\mathbf{X}[a]$ 
 $\mu_1' = \text{mean}(\mathbf{X}')$ 
 $\mathbf{Y}' \leftarrow \emptyset$ 
for pixel  $x$  in  $\mathbf{X}$  do
|  $\mathbf{Y}' \leftarrow D_{MF}(x, \mu_0, \mu_1', \Gamma)$ 
end
return  $\mathbf{Y}'$ 

```

**Algorithm 1:** A two-stage detection algorithm based on the Matched Filter, described in Sec. 2.1.2. In the first stage, Eq. (3) is used to compute detection statistics for pixels. In the second stage a new target spectral signature  $\mu_1'$  is computed as an average of  $N$  highest scoring pixels from Stage 1, and the MF detector is reapplied.

Target spectra in the library were selected to be similar in age to the blood in the image. The approximate age of target spectra is presented in the Tab. 2.

In addition to the experiment with Algorithm 1, three reference experiments were performed for every image by applying the MF detector given by the Eq. 3 with three sources of target (blood) spectra:

1. Spectra from the same spectral library as in the main experiment. This experiment is denoted  $MF_{lib}$  and its result corresponds to the first stage of the Algorithm 1,
2. Mean blood spectra from a different image - this experiment is denoted as the *Inductive MF*,
3. Mean blood spectra from the detected image itself. The experiments is denoted the *Ideal MF* and is similar as in the example in Sec 4.3.

The only parameter of the Algorithm 1, the number of pixels  $N$  used to obtain new target signature in the second stage was set in our experiments to  $N = 1000$ . Sensitivity analysis of this parameter is further discussed in the Sec. 6.1.

### 5.1 Implementation

Experiments were implemented in Python 3.6.9 using libraries: numpy 1.16.4, scipy 1.3.1, scikit-learn 0.22.1, spectral 0.19, matplotlib 3.2.2

Experiments were conducted using a computer with Intel(R) Core i7-5820K CPU @ 330GHz with 64GB of RAM and with the Windows 10 Pro system. The running time of detection algorithms did not exceed tens of seconds.

### 5.2 Results

The aggregated performance of the proposed detection algorithm is presented in Tab. 3 in the form of Area Under Curve (AUC) of

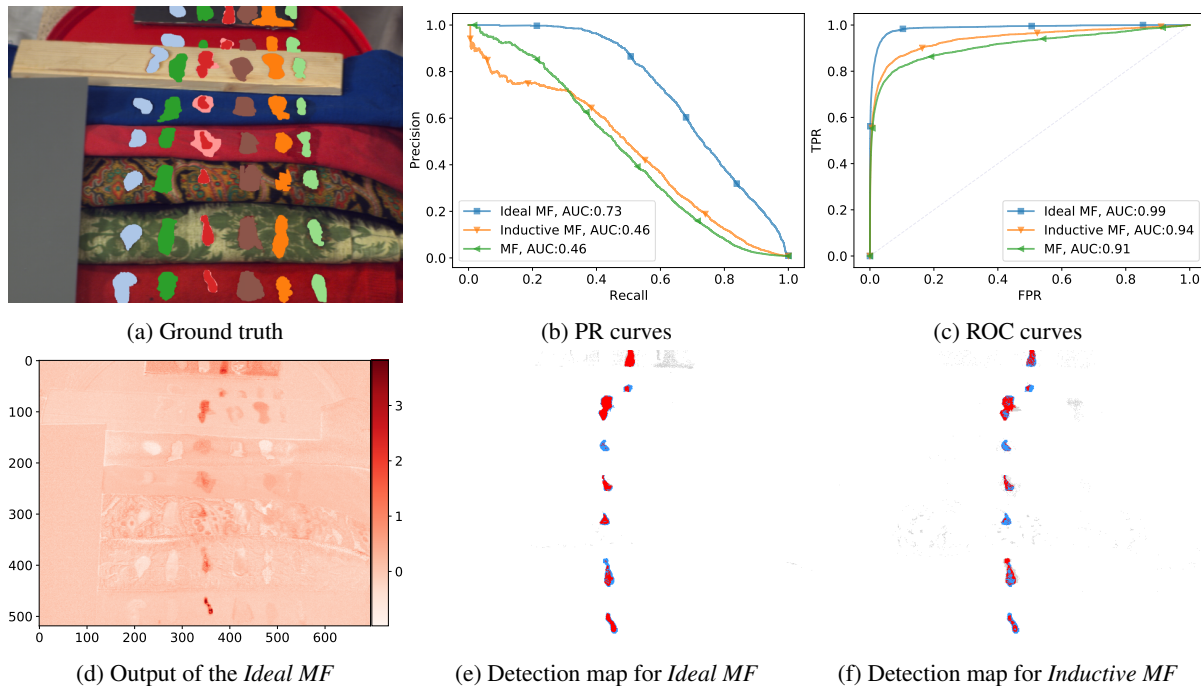


Figure 5: Example: detection performance of three Matched Filter detectors, applied to the scene  $E(1)$ . The *Ideal MF* is trained on blood spectrum from the image itself, the *Inductive MF* on blood from the image  $F(1)$  and the MF on spectrum from the spectral library. Blood class is denoted with red colour in the panel (a). Panels (b) and (c) present PR and ROC curves of the detectors. Panel (d) presents detection score of the *Ideal MF*. The last two panels are detection maps where red colour denotes True Positives (TP), blue colour denotes False negatives (FN) and grey colour denotes False Positives (FP).

Precision-Recall (PR) curves. The table also presents reference results of the MF detector trained on blood pixels from the image itself denoted *Ideal MF*, different image in the dataset denoted *Inductive MF* and the spectral library denoted  $MF_{lib}$ . We can see that results of the *Ideal MF* are high, especially for images from first days. In addition, results of the proposed algorithm and the *Inductive MF* tend to be higher than  $MF_{lib}$ . The higher performance of the Algorithm 1 supports the thesis that the proposed second stage tends to improve the initial detection performance.

Visualisation of detection results for dataset images are presented in Fig. 6, Fig. 7 and Fig. 8. The third column in these figures presents the PR curves that were used to compute AUC values in Tab. 3. The second column in figures presents and example of detection map obtained by setting the threshold  $\eta$  (see Sec. 2) to the actual ratio of blood pixels in the image, i.e.  $\eta = \frac{\text{no. blood pixels}}{\text{no. all pixels}}$ . In other words, for the „oracle” detector this output perfectly matches the ground truth. The output is coloured as follows:

- **Red** colour indicates True Positives (TP): pixels that were correctly detected by the proposed two-stage algorithm. For some images, e.g.  $E(1)$ , this results corresponds quite well to the ground truth, while for other images, such as  $F(1)$ , only a part of the blood splash is detected. However, we can observe that for almost every image and every splash/blob visible in this image at least a subset of pixels in this blob is correctly detected.
- **Orange** colour indicates False Negatives (FN) of the Algorithm 1 which were detected by the *Ideal MF* that uses mean blood spectra from the image itself. Therefore, these pixels could be treated as „potentially detectable” with MF-based algorithm, provided that a proper blood spectrum is available. These pixels are numerous in images where

large blood splashes are present, such as  $E(1)$  or  $A(1)$ .

- **Blue** colour indicates False Negatives (FN) according to both the Algorithm 1 and the *Ideal MF*. We can expect these pixels to be difficult to detect with the MF-based algorithm.
- **Grey** colour indicates False Positives (FP) of the Algorithm 1. We can see that in many images e.g.  $F(1)$ , the *artificial blood* (class 3) is incorrectly detected.
- **Green** colour indicates False Positives (FP) of the *Ideal MF* that were not detected by the proposed algorithm. They often seem to be located in less lit or dark areas (e.g.  $E(1)$ , top of the image) and regions where the *artificial blood* (class 3) is located

## 6 Discussion

Recall that in Tab 3, the second column denoted *Ideal MF* is the performance of the Matched Filter (MF) detector trained on an average target spectrum of the image itself. For the purpose of this discussion, let us assume that this result represents the expected best performance of the MF detector i.e. the „glass ceiling”, reachable with a perfectly matching target spectrum. We notice, that for many images, especially those from first days, e.g.  $F(1)$  or  $A(1)$ , this result is high e.g.  $AUC(PR) \approx 1.0$ . This is confirmed by looking at the visualization e.g. in Fig 6, where unions of sets of red and orange pixels well correspond to location of blood in the image. Looking at the Tab 3 again we notice, that *Ideal MF* results are higher than those from other columns, and in particular results in the column  $MF_{lib}$ . The  $MF_{lib}$  result represents a more „realistic” performance of the detector, obtained by training the MF with spectra from spectral

Table 2: Names and day of acquisition for images in the paper. Codes are unique tags used in the paper. Source image denotes another image in the dataset that was used as a source of blood spectrum in reference experiment. Library index and library age denote the index and age of the blood spectrum from spectral library described in [14]. Image age is the approximate age of target blood in the image.

Image name	Day	Code	Source image	Library index	Library age	Image age
Frame	1	$F(1)$	$F(1a)$	24	1h15	1h20m
Frame	1 (in scene)	$F(1s)$	$F(1a)$	21	3h45m	3h50m
Frame	1 (later)	$F(1a)$	$F(1)$	20	4h50m	5h50m
Frame	2	$F(2)$	$F(1a)$	15	4d	2d
Frame	2 (different camera)	$F(2k)$	$F(2)$	15	4d	2d
Frame	7	$F(7)$	$F(2)$	12	7d	7d
Frame	21	$F(21)$	$F(7)$	5	22d	21d
Splash	1	$D(1)$	$F(1)$	22	2h45m	3h
Head	1	$A(1)$	$F(1)$	21	3h45m	3h30m
Shirt	1	$B(1)$	$F(1s)$	20	4h50m	4h20m
Knife	1	$C(1)$	$F(1)$	21	3h45m	4h
Comparison	1	$E(1)$	$F(1a)$	20	4h50m	4h40m
Comparison	7	$E(7)$	$F(7)$	12	7d	7d
Comparison	21	$E(21)$	$F(21)$	5	22d	21d

Table 3: Aggregated detection performance in experiments expressed as Area Under Curve (AUC) of the Precision-Recall (PR) curve.

Code	<i>Ideal MF</i>	<i>Inductive MF</i>	$MF_{lib}$	Algorithm 1
$F(1)$	1.00	0.41	0.39	0.47
$F(1s)$	1.00	0.92	0.46	0.73
$F(1a)$	1.00	0.17	0.24	0.41
$F(2)$	0.99	0.61	0.37	0.72
$F(2k)$	1.00	0.33	0.41	0.33
$F(7)$	1.00	0.98	0.50	0.83
$F(21)$	1.00	0.98	0.37	0.59
$D(1)$	0.98	0.36	0.28	0.38
$A(1)$	0.97	0.62	0.30	0.30
$B(1)$	0.95	0.31	0.24	0.33
$C(1)$	0.96	0.33	0.34	0.34
$E(1)$	0.73	0.46	0.46	0.71
$E(7)$	0.62	0.26	0.32	0.51
$E(21)$	0.59	0.33	0.29	0.42

library. This difference illustrates the impact of available target spectra on the detection performance. Even for spectra obtained in laboratory conditions and matched in regards to the age of blood, the performance of the MF is significantly lower than its expected best performance.

Following this line of thinking, the difference in results between  $MF_{lib}$  and *Inductive MF* columns in Tab 3 may serve as example of the improvement in performance we can obtain by using a different, more similar target spectra. The *Inductive MF* spectra are taken from a separate image, but since all images in the dataset were acquired in similar environment and with the same equipment, we can expect that they will be more similar to the actual target spectra. Indeed, for many images this is the case e.g. for images  $F(7)$  and  $F(21)$  the result of  $AUC(PR) \approx 0.98$  is close to the expected best detection performance. For some images e.g.  $F(1a)$  the „Inductive” result is lower, but this is probably due to the fact, that  $F(1a)$  and its source image  $F(1)$  were taken during the first few hours after blood application, when the spectra changes resulting from hemoglobin reactions are greatest.

Finally, results of the Algorithm 1, represent the improvement from applying a „local” spectra obtained by averaging a subset of most similar pixels according to the MF detector. We expect, that if the initial detector finds blood in the image, the second stage of the algorithm will allow us to find a more representative blood spectrum. This approach may be perceived as analogous to Machine Learning task of semi-supervised learning, that extends the initial training set with unlabelled data [23]. The visualisation of difference between target spectra in the first and the second stage of the Algorithm 1 is presented in Fig. 9. Results in the Tab 3 suggest, that this idea allows to improve detector’s performance, and in some cases, e.g. for the image  $E(1)$  the result is close to the expected best. However, we notice that the relative difference in performance between the Algorithm 1 and the *Ideal MF* differs for images in the dataset e.g. for the image  $E(1)$  this difference is small and for the image  $F(1)$  it is larger. This subject will be further discussed in the Sec 6.1.



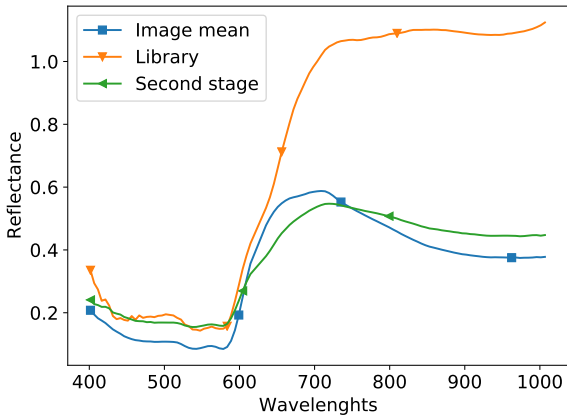


Figure 9: The impact of the second stage of the Algorithm 1 on the target spectrum for the image  $F(I)$ . The „Image mean” denotes the mean blood spectrum in the image, the „Library” denotes the spectrum from the library used in our experiments and the „Second stage” denotes the new blood spectrum used in the second stage of the algorithm.

To summarise, we can say that the Matched Filter detector can achieve high performance in detecting blood, provided that a suitable target spectrum is available. Differences in target spectra may have significant impact on detection performance. However, heuristic methods, such as the Algorithm 1 can often be used to improve the result. An alternative approach could be to use a detector bank, or a form of ensemble, where the final detection would be obtained by combining outputs of multiple detectors with different target spectra.

### 6.1 Sensitivity analysis

Let us compare the performance of the Algorithm 1 for three selected images from our dataset:

- Image  $E(I)$  (Fig. 8, second row): correct detections (red areas) of the Algorithm 1 and the *Ideal MF* are similar. The majority of differences lies in areas of False Positives – the Algorithm 1 incorrectly detects some pixels (grey colour) belonging to one of the fabrics (a camouflage pattern) while the *Ideal MF* detects some pixels (green colour) belonging to the *artificial blood* class. PR curves for both detectors are close together.
- Image  $F(I)$  (Fig. 6, first row): correct detections (red areas) of both algorithms are located mostly on the edges of the blood splash. The rest of the splash is detected only by the *Ideal MF* (orange area), while corresponding detections of the Algorithm 1 are False Positives.
- Image  $A(I)$  (Fig. 7, last row): correct detections (red areas) of both algorithms incorporate the majority of blood splashes on the white fabric in the top area of the image, as well as small subsets of pixels located on large splashes in the bottom. The rest of pixels in these two splashes were detected only by the *Ideal MF*. The difference in performance is also visible in PR curves.

The difference in performance of the Algorithm 1 for the presented three images is clear. For the image Image  $E(I)$  the algorithm’s performance is close to the expected best. For image  $F(I)$  and  $A(I)$  the algorithm detected only a subset of pixels. In addition, as the image  $A(I)$  contains three distinct areas with

blood splashes (splashes in the top, bandage at the bottom, shirt on the left), the majority of pixels detected by the Algorithm 1 were located in the top area.

These differences can be partly attributed to the effect of a second stage of the Algorithm 1 and in particular its parameter  $N$ , which denotes the number of pixels averaged to obtain the new target spectrum. If there is a significant number of pixels in the image where target class is visible, averaging a small subset of best scoring pixels can lead to the situation, when the new target signature becomes representative only for one particular subclass of the target class, such as the top area in the image  $A(I)$ . This suggests that increasing the parameter  $N$  may increase the detector performance. The impact of this parameter is presented in the Fig. 11. As expected, for images where large blood splashes are present, increasing the value of the parameter increases the algorithm’s performance. On the contrary, on images with small number of pixels to detect, small value of the parameter is sufficient.

This leads us to the question, how to estimate the value of the parameter  $N$ ? If we knew the number of target pixels in the image, we could proportionally set the value of the parameter  $N$ , in an analogous way to the detection threshold  $\eta$  (see Sec. 2). Without this knowledge, heuristic estimation of this parameter may be possible, e.g. by analysing histograms of detection output. However, in our opinion such heuristics is beyond the scope of this paper. Therefore, for simplicity, in all our experiments we used a single value of this parameter  $N = 1000$ . As a reference, we provide results for different values of parameter  $N$  in Tab. 4.

Table 4: Performance of the Algorithm 1 expressed as AUC(PR) for different values of the parameter  $N$ . Percentage values are relative to the number of pixels from the target class in the image.

Code	750	1000	10%	20%
$F(I)$	0.46	0.47	0.49	<b>0.51</b>
$F(1s)$	0.81	0.73	<b>0.82</b>	0.63
$F(1a)$	0.39	0.41	0.43	<b>0.43</b>
$F(2)$	0.69	0.72	0.79	<b>0.81</b>
$F(2k)$	0.29	0.33	0.56	<b>0.68</b>
$F(7)$	0.80	0.83	0.90	<b>0.93</b>
$F(21)$	0.53	0.59	0.77	<b>0.82</b>
$D(1)$	0.36	0.38	0.51	<b>0.51</b>
$A(1)$	0.24	0.30	0.40	<b>0.49</b>
$B(1)$	0.34	0.33	0.33	<b>0.34</b>
$C(1)$	0.33	0.34	0.38	<b>0.40</b>
$E(1)$	0.72	0.71	0.72	<b>0.72</b>
$E(7)$	0.54	0.51	<b>0.56</b>	0.55
$E(21)$	0.44	0.42	0.50	<b>0.48</b>

#### 6.1.1 The impact of target class size

Results in Fig. 11 suggest, that while increasing the parameter  $N$  of the Algorithms 1 can significantly increase the detection performance, even for large values of this parameter, this performance is still lower than the expected best result, represented by the *Ideal MF* scores in Tab. 3. This suggests that images with large blood splashes are more difficult for the Algorithms 1. To illustrate this, we performed a complementary detection experiment with Algorithms 1 applied to a modified image  $F(I)$ . The image was modified by cutting a subset of pixels belonging to

the blood class, leaving the rest of the image intact. Result of the experiment are presented in Fig. 10. We can see that results of the Algorithms 1 are inversely proportional to the size of the target class in the image. We can also see that by increasing the value of parameter  $N$ , this effect can be partially compensated.

A similar effect was mentioned in [10], where this performance degradation was attributed to corruption of background covariance matrix by target spectra. Authors suggested that removing best scoring pixels and reapplying the detector may improve its performance. We performed initial experiments and verified that this modification indeed allows to slightly increase the performance of the proposed algorithm. However, since this improvement is minor, and would complicate the algorithm e.g. by introducing another parameter related to the number of ignored pixels, we decided that it is beyond the scope of this paper.

To summarise, the performance of the Algorithm 1 is higher for images where the size of a target class is small. To increase its performance for images with large number of blood pixels, the value of parameter  $N$  should also be increased.

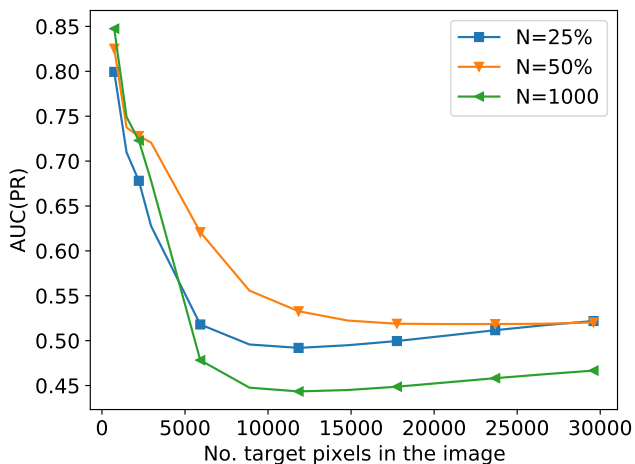


Figure 10: The impact of the number of blood pixels in the image on detection performance. Horizontal axis represents a size of a subset of pixels left in the image  $F(I)$ . Results are presented for three values of parameter  $N$  and represent an average result of five experiments.

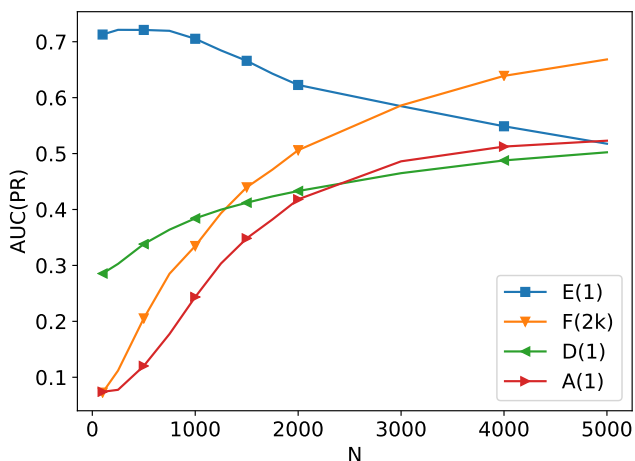


Figure 11: Sensitivity analysis of the Algorithm 1 for selected scenes:  $N$  denotes a number of pixels used for spectra averaging

## 6.2 Class separation for blood and blood-like substances

In our experiments we focused on blood detection and the remaining classes were treated as part of the background and a challenge for the detection algorithm. However, the question arises if the spectra of classes in the image are actually distinctive? To verify this, we selected spectra of blood and blood like substances from scenes  $F(I)$  and  $E(I)$ , and performed a classification experiment. Spectra were randomly, uniformly divided between training and test sets in a stratified way, at a ratio of 5% vectors used for training and 95% for testing. Class 8 ('uncertain blood') was removed. Such data was classified using the SVM [24] classifier with RBF kernel. Parameters were chosen through internal cross-validation from a range of  $C \in \langle 10^{-2}, 10^2 \rangle$  and  $\gamma \in \langle s \times 10^{-2}, s \times 10^2 \rangle$ , where  $s = \frac{1}{(N_f * V)}$ ,  $N_f$  is the number of features and  $V$  is the variance of data. The experiment was repeated 10 times. For the scene  $E(I)$  we obtained accuracy score of  $97.8\% \pm 0.23$ . When performing binary classification between blood and non-blood, the precision score of  $98.49\% \pm 0.86$  and the recall score of  $94.83\% \pm 1.92$  were obtained. For the scene  $F(I)$  almost no errors were made. The experiment confirms that the classes can be well modelled with ML algorithms and are distinguishable.

We note that this classification scenario is used for illustration of dataset properties and is different from the detection scenario used in the rest of our experiments. For instance, the classifier deals only with annotated classes (the rest of the background is ignored) and the training set, while separate from the test set, is sampled from the same image. This is why the accuracy of the classifier is so high.

## 7 Conclusions

We presented a diverse dataset aimed to facilitate the development of blood detection algorithms in hyperspectral images. In order to explore this dataset, we approached the task of blood detection from the perspective of hyperspectral target detection. This allowed us to apply well-understood statistical detectors and observe their performance for different images in the dataset. In our opinion this approach is more general than a dedicated algorithm focused e.g. on detection of characteristic bands, while at the same time it provides a logical reference for more specialised methods.

Our results show that blood is spectrally distinct and can be quite reliably detected when a matching set of training examples is available. However, spectra changes induced by ageing of the blood and the fact that spectra are mixed with unknown background can make finding such training set a challenging task. This problem can be approached with heuristic approaches, in a similar way to the detection algorithm presented in our experiment. A possible extension of this approach would be to use spatial-spectral processing in order to make use of the fact that blood pixels can be expected to from spatial groups as e.g. in [23]. Another approach would be to employ mixing models as e.g. in [13] in order to extract haemoglobin endmembers.

We also believe that the proposed dataset can be an interesting case for the development of classification algorithms. While we discussed a simple experiment where a classifier is used to distinguish between annotated classes in one of the images, the development of an „inductive” classifier trained on one image and tested on others is a more challenging task.

## 8 Acknowledgements

Authors would like to thank Paulina Krupska and Joanna Sobczyk for carrying out reference measurements using the hyperspectral imaging system and the spectrometer. In addition, the Laboratory of Analysis and Nondestructive Investigation of Heritage Objects (LANBOZ) at the National Museum in Krakow is acknowledged for allowing the authors to use their SPECIM hyperspectral cameras. Authors would also like to thank Alicja Majda for making available the spectral library described in [14].

## References

- [1] Grzegorz Zadora and Alicja Menzyk. In the pursuit of the holy grail of forensic science-spectroscopic studies on the estimation of time since deposition of bloodstains. *TrAC Trends in Analytical Chemistry*, 2018.
- [2] Stuart H James and Jon J Nordby. *Forensic science: an introduction to scientific and investigative techniques*. CRC press, 2002.
- [3] Bruce Budowle, Jeffrey L Leggitt, Debra A Defenbaugh, Kathleen M Keys, and Steven F Malkiewicz. The presumptive reagent fluorescein for detection of dilute bloodstains and subsequent str typing of recovered dna. *Journal of forensic science*, 45(5):1090–1092, 2000.
- [4] Filippo Barni, Simon W Lewis, Andrea Berti, Gordon M Miskelly, and Giampietro Lago. Forensic application of the luminol reaction as a presumptive test for latent blood detection. *Talanta*, 72(3):896–913, 2007.
- [5] Dimitris Manolakis, David Marden, Gary A Shaw, et al. Hyperspectral image processing for automatic target detection applications. *Lincoln laboratory journal*, 14(1):79–116, 2003.
- [6] Prasad S Thenkabail and John G Lyon. *Hyperspectral remote sensing of vegetation*. CRC Press, 2016.
- [7] Yuan-Yuan Pu, Yao-Ze Feng, and Da-Wen Sun. Recent progress of hyperspectral imaging on quality and safety inspection of fruits and vegetables: a review. *Comprehensive Reviews in Food Science and Food Safety*, 14(2):176–188, 2015.
- [8] Bartosz Grabowski, Wojciech Masarczyk, Przemysław Głomb, and Agata Mendys. Automatic pigment identification from hyperspectral data. *Journal of Cultural Heritage*, 31:1–12, 2018.
- [9] Przemysław Głomb, Michał Romaszewski, Michał Cholewa, and Krzysztof Domino. Application of hyperspectral imaging and machine learning methods for the detection of gunshot residue patterns. *Forensic science international*, 290:227–237, 2018.
- [10] Dimitris Manolakis, Ronald Lockwood, Thomas Cooley, and John Jacobson. Is there a best hyperspectral detection algorithm? In *Algorithms and technologies for multispectral, hyperspectral, and ultraspectral imagery XV*, volume 7334, page 733402. International Society for Optics and Photonics, 2009.
- [11] Guolan Lu and Baowei Fei. Medical hyperspectral imaging: a review. *Journal of biomedical optics*, 19(1):010901, 2014.
- [12] WG Zijlstra and A Buursma. Spectrophotometry of hemoglobin: absorption spectra of bovine oxyhemoglobin, deoxyhemoglobin, carboxyhemoglobin, and methemoglobin. *Comparative Biochemistry and Physiology Part B: Biochemistry and Molecular Biology*, 118(4):743–749, 1997.
- [13] Martin H Skjelvareid, Karsten Heia, Stein Harris Olsen, and Svein Kristian Stormo. Detection of blood in fish muscle by constrained spectral unmixing of hyperspectral images. *Journal of Food Engineering*, 212:252–261, 2017.
- [14] Alicja Majda, Renata Wietecha-Posłuszny, Agata Mendys, Anna Wójtowicz, and Barbara Łydźba-Kopczyńska. Hyperspectral imaging and multivariate analysis in the dried blood spots investigations. *Applied Physics A*, 124(4):312, 2018.
- [15] Gerda Edelman, Vicky Manti, Saskia M van Ruth, Ton van Leeuwen, and Maurice Aalders. Identification and age estimation of blood stains on colored backgrounds by near infrared spectroscopy. *Forensic science international*, 220(1-3):239–244, 2012.
- [16] G.J. Edelman, E. Gaston, T.G. van Leeuwen, P.J. Cullen, and M.C.G. Aalders. Hyperspectral imaging for non-contact analysis of forensic traces. *Forensic Science International*, 223(1):28 – 39, 2012.
- [17] Jie Yang, Jobin J Mathew, Roger R Dube, and David W Messinger. Spectral feature characterization methods for blood stain detection in crime scene backgrounds. In *Algorithms and Technologies for Multispectral, Hyperspectral, and Ultraspectral Imagery XXII*, volume 9840, page 98400E. International Society for Optics and Photonics, 2016.
- [18] Gerarda Johanna Edelman et al. *Spectral analysis of blood stains at the crime scene*. PhD thesis, Faculty of Medicine, University of Amsterdam, 2014.
- [19] Jie Yang, David W Messinger, Jobin J Mathew, and Roger R Dube. Comparison of algorithms for blood stain detection applied to forensic hyperspectral imagery. In *Algorithms and Technologies for Multispectral, Hyperspectral, and Ultraspectral Imagery XXII*, volume 9840, page 98400X. International Society for Optics and Photonics, 2016.
- [20] Bo Li, Peter Beveridge, William T O’Hare, and Meez Islam. The application of visible wavelength reflectance hyperspectral imaging for the detection and identification of blood stains. *Science & justice*, 54(6):432–438, 2014.
- [21] Yuefeng Zhao, Nannan Hu, Yunuan Wang, Yonglei Liu, Xiaofei Li, and Jingjing Wang. The application of near-infrared reflectance hyperspectral imaging for the detection and extraction of bloodstains. *Cluster Computing*, 22(4):8453–8461, 2019.
- [22] Jesse Davis and Mark Goadrich. The relationship between precision-recall and roc curves. In *Proceedings of the 23rd international conference on Machine learning*, pages 233–240, 2006.

- [23] Michał Cholewa, Przemysław Głomb, and Michał Romaszewski. A spatial-spectral disagreement-based sample selection with an application to hyperspectral data classification. Accepted for publication in *Geoscience and Remote Sensing Letters*, 2018.
- [24] Farid Melgani and Lorenzo Bruzzone. Classification of hyperspectral remote sensing images with Support Vector Machines. *IEEE Transactions on geoscience and remote sensing*, 42(8):1778–1790, 2004.



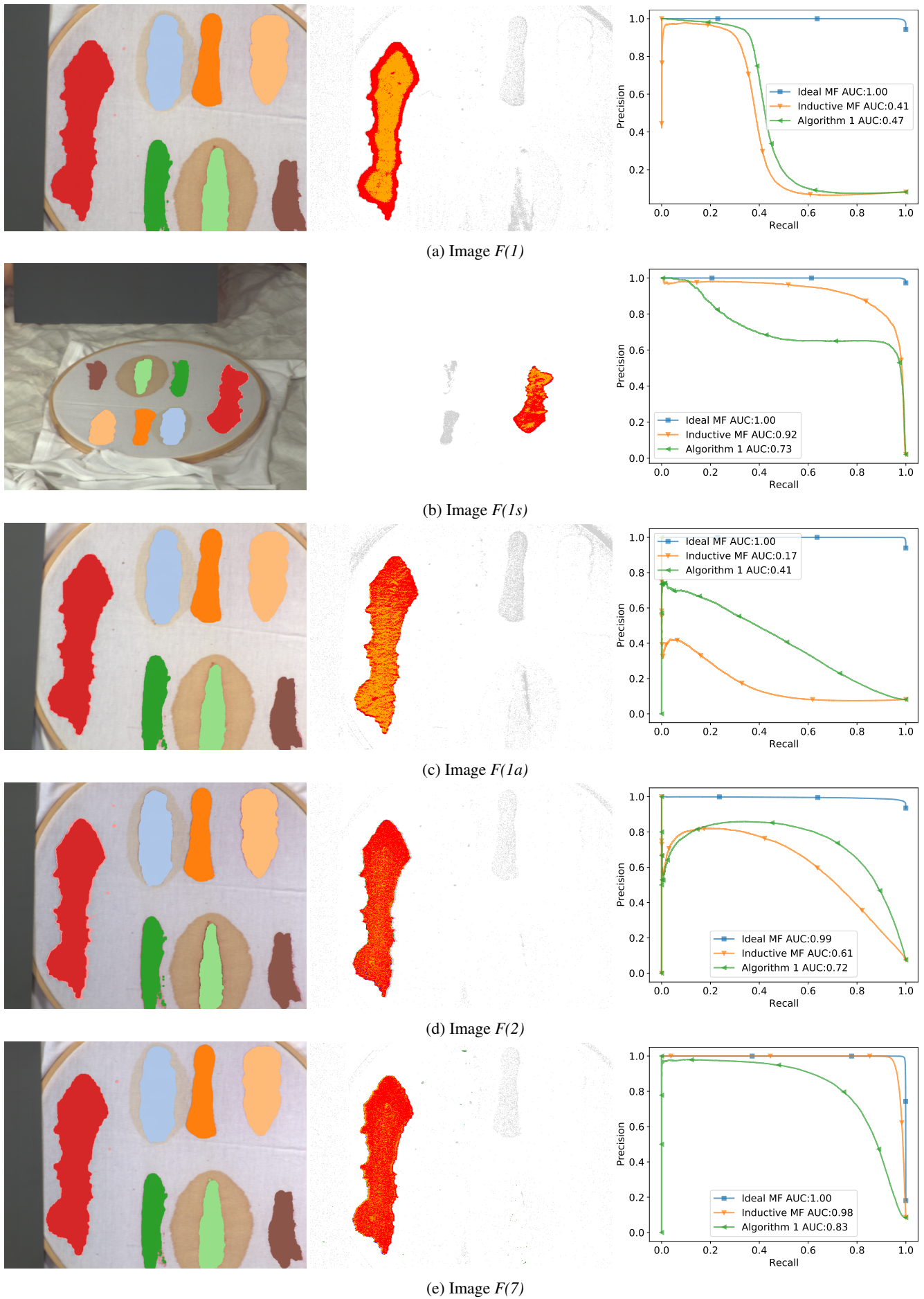


Figure 6: Performance of the Algorithm 1 for dataset images. Left column is ground truth—blood is denoted with red colour. Middle column is the coloured example output of the detector—correct detections (TP) are coloured red, potential detections (FN of the Algorithm 1 but TP of the *Ideal MF*) are coloured orange, incorrect detections (FP) are coloured grey. The last column presents PR curves for the Algorithm 1, the *Inductive MF* and the *Ideal MF*.

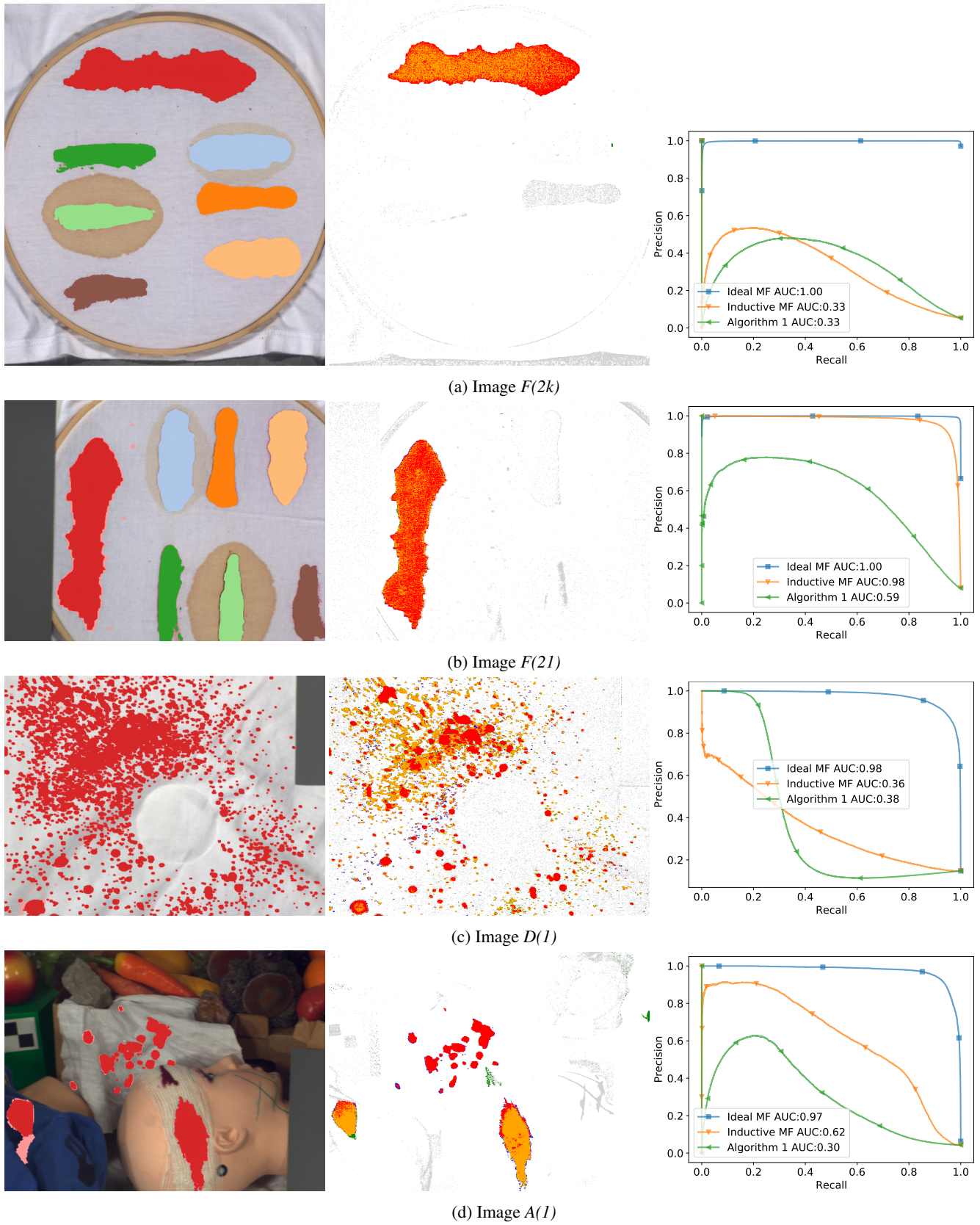


Figure 7: Performance of the Algorithm 1 for dataset images. Left column is ground truth—blood is denoted with red colour. Middle column is the coloured example output of the detector—correct detections (TP) are coloured red, potential detections (FN of the Algorithm 1 but TP of the *Ideal MF*) are coloured orange, incorrect detections (FP) are coloured grey. The last column presents PR curves for the Algorithm 1, the *Inductive MF* and the *Ideal MF*.



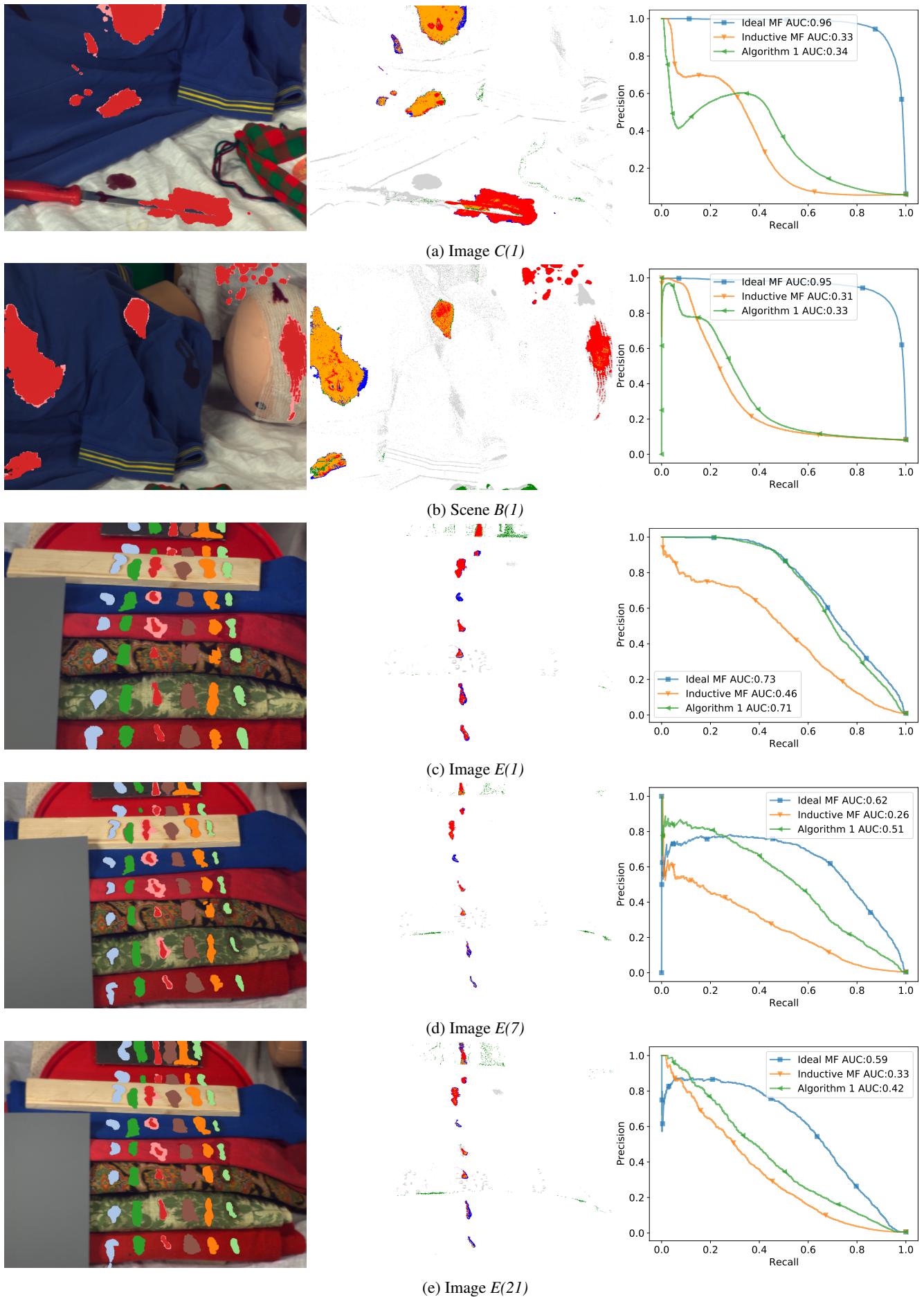


Figure 8: Performance of the Algorithm 1 for dataset images. Left column is ground truth—blood is denoted with red colour. Middle column is the coloured example output of the detector—correct detections (TP) are coloured red, potential detections (FN of the Algorithm 1 but TP of the *Ideal MF*) are coloured orange, incorrect detections (FP) are coloured grey. The last column presents PR curves for the Algorithm 1, the *Inductive MF* and the *Ideal MF*.